Resonant inelastic x-ray scattering study of $Bi_6Fe_2Ti_3O_{18}$, $Bi_6FeCoTi_3O_{18}$, and $LaBi_5FeCoTi_3O_{18}$ Aurivillius-phase oxides

Zhangzhang Cui,[1,2] Xiaofang Zhai,[1,2] Yi-De Chuang,[3] Hui Xu,[1] Haoliang Huang,[1,2] Jianlin Wang,[2,4] Zhengping Fu,[1,2] Ranran Peng,[1,2] Jinghua Guo,[3,5,*] and Yalin Lu[1,2,4,6,†]

[1]*Hefei National Laboratory for Physical Sciences at the Microscale and Department of Materials Science and Engineering, University of Science and Technology of China, Hefei 230026, Anhui, China*

[2]*Synergetic Innovation Center of Quantum Information and Quantum Physics, University of Science and Technology of China, Hefei 230026, Anhui, China*

[3]*Advanced Light Source, Lawrence Berkeley National Laboratory, Berkeley, California 94720, USA*

[4]*National Synchrotron Radiation Laboratory, University of Science and Technology of China, Hefei 230026, Anhui, China*

[5]*Department of Chemistry and Biochemistry, University of California, Santa Cruz, California 95064, USA*

[6]*Laser Optics Research Center, Department of Physics, United States Air Force Academy, Colorado Springs, Colorado 80840, USA*

(Received 30 November 2016; revised manuscript received 10 April 2017; published 3 May 2017)

Aurivillius-phase oxides exhibit the coexistence of ferroelectricity (FE) and ferromagnetism (FM) above room temperature, and the FE and FM orders can be modified by various dopants. However, detailed examinations of their electronic structures in response to the dopants are still lacking. Here, the $Bi_6Fe_2Ti_3O_{18}$, $Bi_6FeCoTi_3O_{18}$, and $LaBi_5FeCoTi_3O_{18}$ epitaxial thin films were prepared and the systematic experimental and theoretical resonant inelastic x-ray scattering (RIXS) studies were performed at both Fe and Co L edges. The RIXS measurements reveal the modified electronic structures induced by the doping of Co and La. The RIXS simulations demonstrate that the electronic structure variations are the outcome of modified crystal-field parameters of FeO_6 and CoO_6 octahedra.

DOI: 10.1103/PhysRevB.95.205102

I. INTRODUCTION

Aurivillius-phase oxides that exhibit the coexistence of ferroelectricity (FE) and ferromagnetism (FM) above room temperature have drawn intensive attention in recent years [1–4]. The basic building blocks of these oxides are the oxygen octahedra. Numerous novel physical properties associated with oxygen octahedra are of great interest in condensed matter physics. For instance, the rotation of oxygen octahedra (OOR) can be related to magnetism, improper ferroelectricity, and emergent electronic properties in artificial superlattices or heterostructures [5–8]. Such rotation is a pure elastic distortion. Deformation of oxygen octahedra is another type of distortion commonly seen in perovskite oxides. This type of distortion can be induced by the Jahn-Teller effect, element doping, or even lattice defects such as oxygen vacancies [9–12]. A careful study of electronic structures associated with oxygen octahedra can greatly benefit the understanding of physical properties of perovskite oxides.

Synchrotron-based soft x-ray spectroscopies have been extensively used to investigate the electronic structures of a wide range of materials. Among these spectroscopies, resonant inelastic x-ray scattering (RIXS) in particular can offer the unique opportunity to reveal the response of electronic structures to the distortion of oxygen octahedra: In oxygen octahedra, the transition-metal d orbitals hybridize with oxygen $2p$ orbitals; the crystal field imposed on central transition-metal ions depends on the geometric configuration of oxygen octahedra, which in turns influences the electronic states of the transition-metal d electrons. RIXS has been used extensively in studying the excitations between transition-metal d electrons (d-d excitations) or between oxygen $2p$ and transition-metal d orbitals (charge-transfer excitations) [13,14].

In this work, we have performed comprehensive RIXS studies on Aurivillius-phase oxides [general formula $(Bi_2O_2)^{+2}(A_{n-1}B_nO_{3n+1})^{-2}$, A = Bi, La, Sr, etc.; B = Ti, Fe, Co, etc.; and n is the number of perovskitelike layers] to investigate their electronic structures in response to dopants. $Bi_6Fe_2Ti_3O_{18}$ (BFTO) is specifically chosen as the parent compound. BFTO has a unique perovskite layer structure and is flexible for doping with various elements [15–17]. Doping Co (B-site doping) and La (A-site doping) into BFTO can introduce an enhanced ferromagnetism above room temperature in $Bi_6FeCoTi_3O_{18}$ (BFCTO) and $LaBi_5FeCoTi_3O_{18}$ (LBFCTO) [17–21]. The presence of weak ferromagnetism in these compounds is believed to originate from the canting of Fe and Co spins via Dzyaloshinskii-Moriya (DM) interaction associated with lattice distortion [15,18]. However, experimental confirmations of such lattice distortion are still inconclusive [21]. Herein, the RIXS measurements at both Fe and Co L edges on BFTO, BFCTO, and LBFCTO epitaxial thin films are performed and the results are compared with the atomic multiplet plus crystal-field simulations. The combined experimental and simulated RIXS studies provide the clear evidence of modified crystal-field parameters induced by the doping of Co and La.

II. EXPERIMENT

High-quality $Bi_6Fe_2Ti_3O_{18}$, $Bi_6FeCoTi_3O_{18}$, and $LaBi_5FeCoTi_3O_{18}$ thin films were epitaxially grown on (0 0 1) oriented $(LaAlO_3)_{0.3}(Sr_2AlTaO_6)_{0.7}$ (LSAT) substrates with $LaNiO_3$ (LNO) buffer layers using the pulsed laser

*jguo@lbl.gov
†yllu@ustc.edu.cn

deposition (PLD) method. The preparation procedures for BFCTO and LBFCTO films were reported previously [21]. The BFTO films were deposited at 830 °C using similar procedures as those of BFCTO and LBFCTO. The crystalline structures of these films were characterized by Rigaku four-circle x-ray diffraction (XRD) diffractometer. The soft x-ray absorption (XAS) and resonant inelastic x-ray scattering spectroscopy measurements were performed on beamlines 4.0.3, 6.3.1.2, and 8.0.1 at the Advanced Light Source, Lawrence Berkeley National Laboratory. The energy resolution for Fe and Co L-edge XAS is about 0.2 eV and the combined energy resolution for RIXS determined from the full width at half maximum (FWHM) of the elastic peak is about 0.7 eV. During XAS and RIXS measurements, the incident beam was at 45° relative to the surface normal of the thin films. For RIXS measurements, the incident photons were polarized linearly in the horizontal scattering plane (π polarization) and the scattered photons were collected by the spectrometer mounted at 90° emission angle relative to the incident beam.

III. RESULTS AND DISCUSSION

A. XRD characterizations

The crystalline structures of BFTO, BFCTO, and LBFCTO films characterized by XRD ω-2θ scans (Fig. 1) exhibit the typical $n = 5$ Aurivillius-phase structure. All diffraction peaks can be assigned to the (0 0 L) index. No other impurity peaks are observed in the plot, suggesting that the films are all c-axis oriented. The thickness of films determined from the reflection fringes is around 41, 66, and 44 nm for BFTO, BFCTO, and LBFCTO, respectively. The out-of-plane lattice constants for BFTO, BFCTO, and LBFCTO films are calculated to be 49.7 ± 0.1 Å, 49.5 ± 0.5 Å, and 49.2 ± 0.2 Å, respectively.

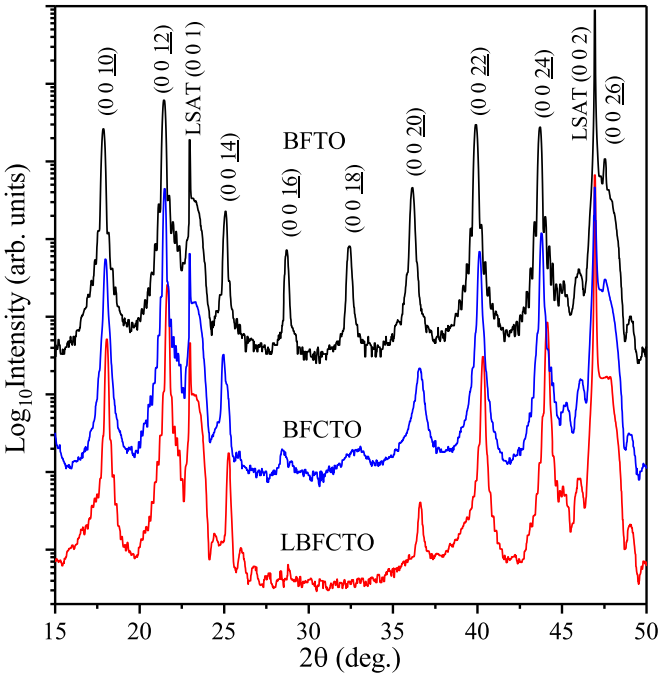

FIG. 1. XRD ω-2θ scans of BFTO (top, black), BFCTO (middle, blue), and LBFCTO (bottom, red) films.

In bulk phase, the BFTO, BFCTO, and LBFCTO are in the orthorhombic structure at room temperature, while their epitaxial thin films are coherently strained to the substrates as confirmed from the XRD reciprocal space maps of our previous reports [21,22]. This means the BFTO, BFCTO, and LBFCTO films are in the tetragonal structure due to interface strain. The decrease in the out-of-plane lattice constants could be related to the distortion of $(Fe/Co/Ti)O_6$ octahedra along the c axis. With Co and La doping, the (0 0 16) and (0 0 18) peaks of BFCTO are much weaker than that of BFTO, and finally disappear in the XRD of LBFCTO. These observations indicate that the long-range order of superlattice structure is disturbed by the lattice distortion, presumably introduced by Co and La doping.

B. Fe and Co L-edge XAS measurements

The modifications of electronic structures by the doping of Co and La are studied using near-edge XAS and RIXS spectroscopies at both Fe and Co sites. Figure 2(a) shows Fe L-edge XAS spectra of BFTO, BFCTO, and LBFCTO films. Two groups of peaks around 708 eV (L_3) and 721 eV (L_2) are due to the transitions from spin-orbit-split Fe $2p$ core levels to the unoccupied Fe $3d$ orbitals [23,24]. The two peaks within each group come from the interplay of

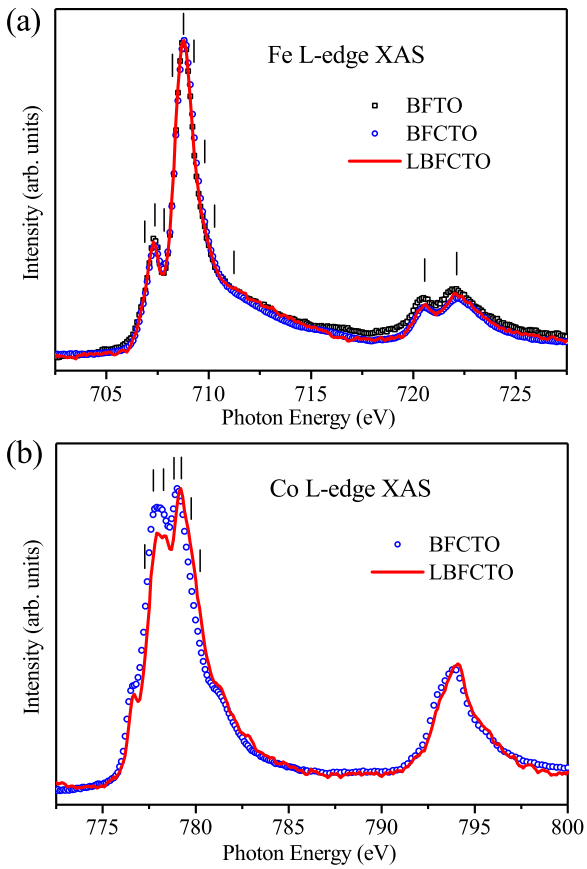

FIG. 2. (a) Fe L-edge XAS spectra of BFTO (open square, black), BFCTO (open circle, blue), and LBFCTO (solid line, red) films. (b) Co L-edge XAS spectra of BFCTO (open circle, blue) and LBFCTO (solid line, red) films. All XAS spectra are normalized to the incident photon flux and maximum intensity. The vertical bar indicates the excitation energies used in the following RIXS spectra.

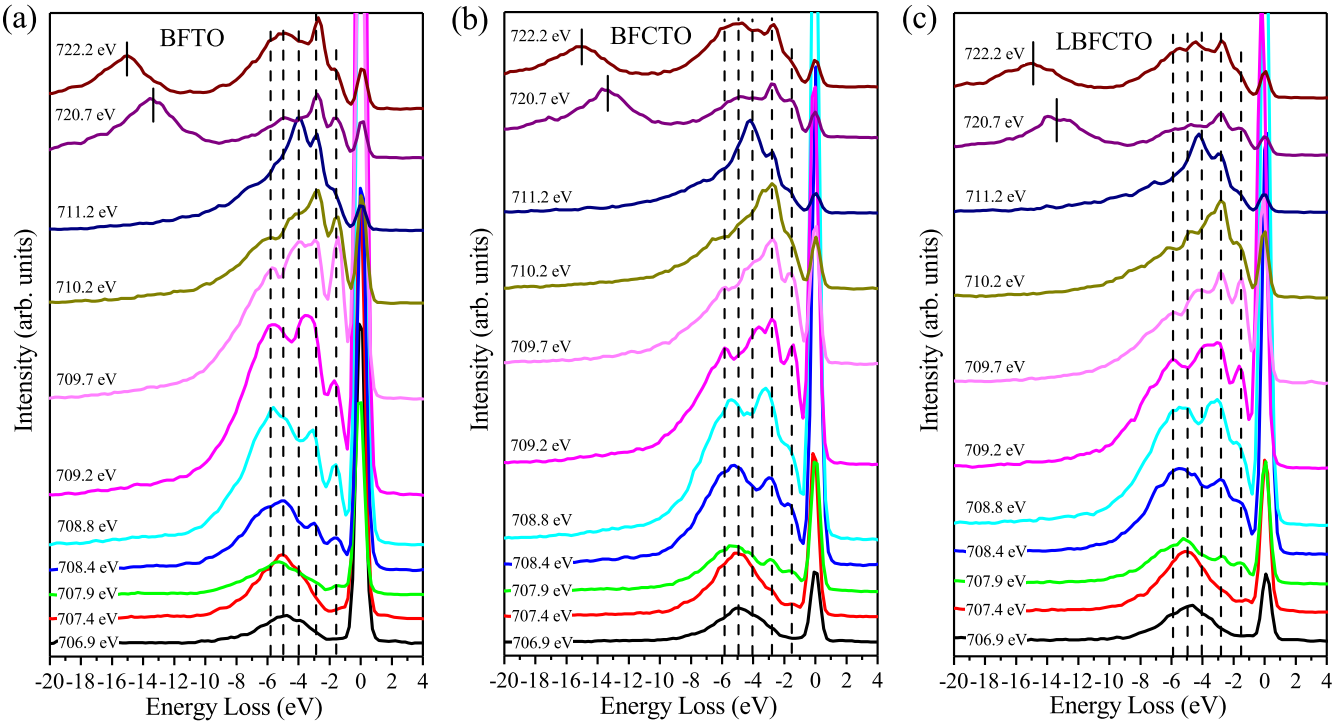

FIG. 3. Fe L-edge RIXS spectra of (a) BFTO, (b) BFCTO, and (c) LBFCTO films at selected incident photon energies. The incident photon energies are displayed next to the corresponding RIXS spectra and are indicated by vertical sticks in Fig. 2(a).

crystal-field splitting, charge transfer, and p-d/d-d Coulomb and exchange interactions [24]. The Coulomb and exchange interactions result in the multiplet states within the edges and the crystal field formed by oxygen ions further splits the multiplets. The charge transfer can also split the d levels and lead to asymmetric spectral shape, which is present at the higher-energy side of the main absorption peak at 709 eV [24]. The Fe L-edge XAS spectra of all films are quite similar without discernible differences. By comparing with FeO and α-Fe_2O_3 reference spectra [21], the spectral shape of the films bears similarity to that of α-Fe_2O_3, suggesting that the Fe ions are in a 3+ valence state in all films.

Figure 2(b) shows Co L-edge XAS spectra of BFCTO and LBFCTO films. Similar to the XAS of Fe, two absorption edges from spin-orbit-split Co $2p$ core levels can be observed around 778 eV (L_3) and 794 eV (L_2) [25,26]. Strong multiplet effects due to Coulomb and exchange interactions are observed at the L_3 absorption edge. By comparing with CoO and $LaCoO_3$ reference spectra [21], the valence states of Co in both films are confirmed to be closer to 2+ with a small Co^{3+} contribution. The 2+ valence state for Co is due to the presence of oxygen vacancies in these compounds, which is very common in Aurivillius-phase oxides. Moreover, Co ions in the LBFCTO film exhibit slightly higher valency than in the BFCTO film [21]. The increase in Co valency can be attributed to the decrease of oxygen vacancy concentration due to the reduced evaporation of Bi by La substitution [17].

C. Fe and Co L-edge RIXS measurements

Although the electronic structures of films can be investigated using XAS, the core-hole lifetime broadening in the XAS process prohibits us from carefully examining the spectroscopic response to the dopants. RIXS is a second-order optical process and its energy resolution is not limited by the core-hole lifetime [27]. Thus the fine electronic states of Fe and Co $3d$ electrons under the oxygen octahedral crystal field can be well studied using RIXS.

Figure 3 shows the Fe L-edge RIXS spectra of BFTO, BFCTO, and LBFCTO films at several selected incident photon energies spanning over both L_3 and L_2 edges. The RIXS spectra are all normalized to incident photon flux with the same acquisition time (30 min for each spectrum) and shown on the energy loss scale. Strong resonance can be observed when varying the incident photon energy across the absorption edges. The spectral structures can basically be divided into three categories: the elastic lines at zero energy loss coming from the recombination of the $2p^5 3d^6$ intermediate state to the ground state (Rayleigh scattering); the resonant features at nonzero energy loss due to d-d excitations, charge-transfer excitations, etc. (RIXS); the normal x-ray emission lines from the decay of electrons in Fe^{3+} $3d$ occupied states into $2p_{1/2}$ and $2p_{3/2}$ core holes. In the RIXS spectra, the two loss peaks at -13.5 and -15 eV (indicated by vertical sticks) are due to Fe^{3+} L_3 normal emissions. In addition to the elastic and normal emission features, five loss peaks at the energy range from -1 to -10 eV are well resolved (indicated by dashed lines). The Fe L-edge RIXS spectra are similar to previous reports on a series of compounds [24,28–30], except we notice that our RIXS spectra exhibit much stronger elastic peaks that resonate strongly with the incident photon energy. This is probably due to scattering from the surface of very-high-quality thin films in specular geometry employed in the RIXS measurements. Our RIXS data also agree nicely

TABLE I. Energies of Fe^{3+} L-edge RIXS excitations and the corresponding transitions.

Energy loss (eV)	Assigned transitions
−1.6	$^6A_1 \rightarrow {}^4E$
−2.8	$3e_g \uparrow \rightarrow 3e_g \downarrow$
−4.0	$1t_{1u} \downarrow \rightarrow 2t_{2g} \downarrow$
−5.0	$1t_{1g} \downarrow \rightarrow 3e_g \downarrow$
−5.8	$6t_{1u} \downarrow \rightarrow 3e_g \downarrow$

with the optical absorption studies of α-Fe_2O_3 [31]. Based on these studies, the first loss peak at −1.6 eV is due to $^6A_1 \rightarrow {}^4E$ crystal-field transitions; the second loss peak around −2.8 eV could be assigned to the spin-flip transitions among $3e_g$ states; the other three loss peaks around −4, −5, and −5.8 eV can be attributed to the $O^{2-} \rightarrow Fe^{3+}$ charge-transfer transitions [31]. These transitions are also summarized in Table I.

The Fe L-edge RIXS spectral shapes of BFTO, BFCTO, and LBFCTO films are quite similar and the energy positions of loss features do not show notable changes. However, close examination shows that the relative intensities of these excitations, especially the first and second loss peaks, exhibit significant differences. Upon the substitution of Co to Fe sites, the $^6A_1 \rightarrow {}^4E$ transition in the BFCTO film shows a decrease in relative intensity compared to the BFTO film, while with the doping of La, the relative intensity of this transition in the LBFCTO film shows an increase compared to the BFCTO film, but still weaker than that of the BFTO film. This finding will be further examined by atomic multiplet simulations of Fe^{3+} L-edge RIXS.

Figure 4 shows Co L-edge RIXS spectra of BFCTO and LBFCTO films at several selected incident photon energies across the Co L_3 edge. The RIXS data are all normalized to incident photon flux with the same acquisition time (10 min for each spectrum), and shown on an energy loss scale. The Co L-edge RIXS spectra of BFCTO and LBFCTO films are quite similar to that of CoO reported previously [25,32], indicating that we can interpret the Co RIXS data of the films based on

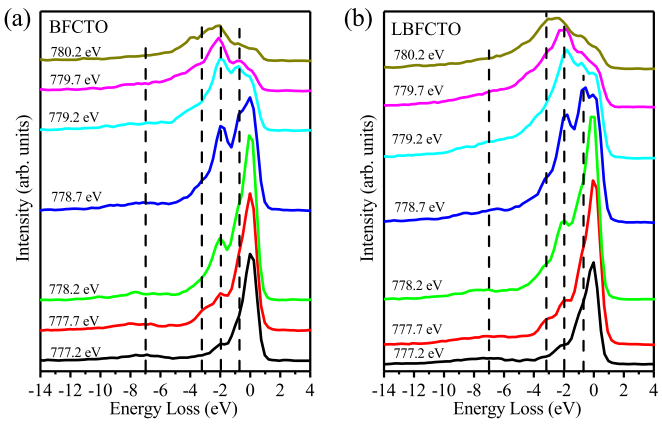

FIG. 4. Co L-edge RIXS spectra of (a) BFCTO and (b) LBFCTO films at selected incident photon energies. The incident photon energies are displayed next to the corresponding RIXS spectra and are indicated by vertical sticks in Fig. 2(b).

TABLE II. Energies of Co^{2+} L-edge RIXS excitations and the corresponding transitions.

Energy loss (eV)	Assigned transitions
−0.7	$^4T_{1g}(^4F) \rightarrow {}^4T_{2g}(^4F)$
−2.0	$^4T_{1g}(^4F) \rightarrow {}^4A_{2g}(^4F) + {}^4T_{1g}(^4P)$
−3.2	$^4T_{1g}(^4F) \rightarrow {}^2E_g$

the studies of CoO. The RIXS spectra exhibit four distinct loss peaks that arise from d-d and charge-transfer excitations. If we do not take into account the small distortion of CoO_6 octahedra, under octahedral symmetry (O_h), the first loss peak at −0.7 eV can be assigned to d-d transition $^4T_{1g}(^4F) \rightarrow {}^4T_{2g}(^4F)$, and the second loss peak at −2.0 eV is from the overlapping of $^4T_{1g}(^4F) \rightarrow {}^4A_{2g}(^4F)$ and $^4T_{1g}(^4F) \rightarrow {}^4T_{1g}(^4P)$ transitions; the weak loss peak around −3.2 eV is due to transitions from the $^4T_{1g}(^4F)$ ground state to, among others, the ^2E_g multiplet states [32]. The assignments of these d-d excitations are also summarized in Table II. The broad dispersion around −7 eV can be attributed to O $2p$ to Co $3d$ charge-transfer excitations [25,26]. The crystal-field splitting energy $10Dq$ of BFCTO and LBFCTO films can be determined to be about 0.7 eV from the energy position of the first loss peak [32,33]. Though there is no discernible difference between the energy of d-d excitations, we observe an abrupt increase in the intensity of the $^4T_{1g}(^4F) \rightarrow {}^4T_{2g}(^4F)$ transition in the RIXS spectrum of the LBFCTO film at 778.7 eV excitation energy.

D. Fe and Co L-edge RIXS and XAS simulations

In order to elucidate the intensity behavior of Fe and Co RIXS spectra, we have performed RIXS simulations using the atomic multiplet code (CTM4XAS + CTM4RIXS) developed by de Groot and co-workers [34]. The simulation method and energetic values of simulation parameters can also be found in Refs. [32,33]. For the RIXS simulations of both Fe^{3+} and Co^{2+}, the Slater integral (to account for Coulomb and exchange interactions of $2p$ and $3d$ electrons) and spin-orbit coupling are reduced to 60% and 80% of their Hartree-Fock values, respectively. The Lorentzian function that is used to account for the $2p$ core-hole lifetime broadening is set to 0.2 eV for both Fe and Co. The Gaussian function used for experimental resolution is set to 0.7 and 0.2 eV for Fe and Co, respectively. The simulated Co RIXS spectra are not broadened with the experimental resolution so that they can show more details and richer structures. The simulations are performed using the experimental scattering geometry and D_{4h} symmetry. The FeO_6 octahedra may be in a lower symmetry group than D_{4h} [35]. This requires further crystal-field splitting to be added in the atomic multiplet code, which is currently unavailable. We would like to emphasize that as the BFTO, BFCTO, and LBFCTO films have a unique layer structure and tetragonal lattice, the actual crystalline structures of FeO_6 and CoO_6 octahedra should be close to D_{4h}. Although there is a small contribution of Co^{3+} in BFCTO and LBFCTO films, for simplicity, we have assumed that the Co ions are in a 2+ valence state. In FeO_6 and CoO_6 octahedra, the Fe^{3+} and Co^{2+} $3d$ electronic states can be strongly modulated by the

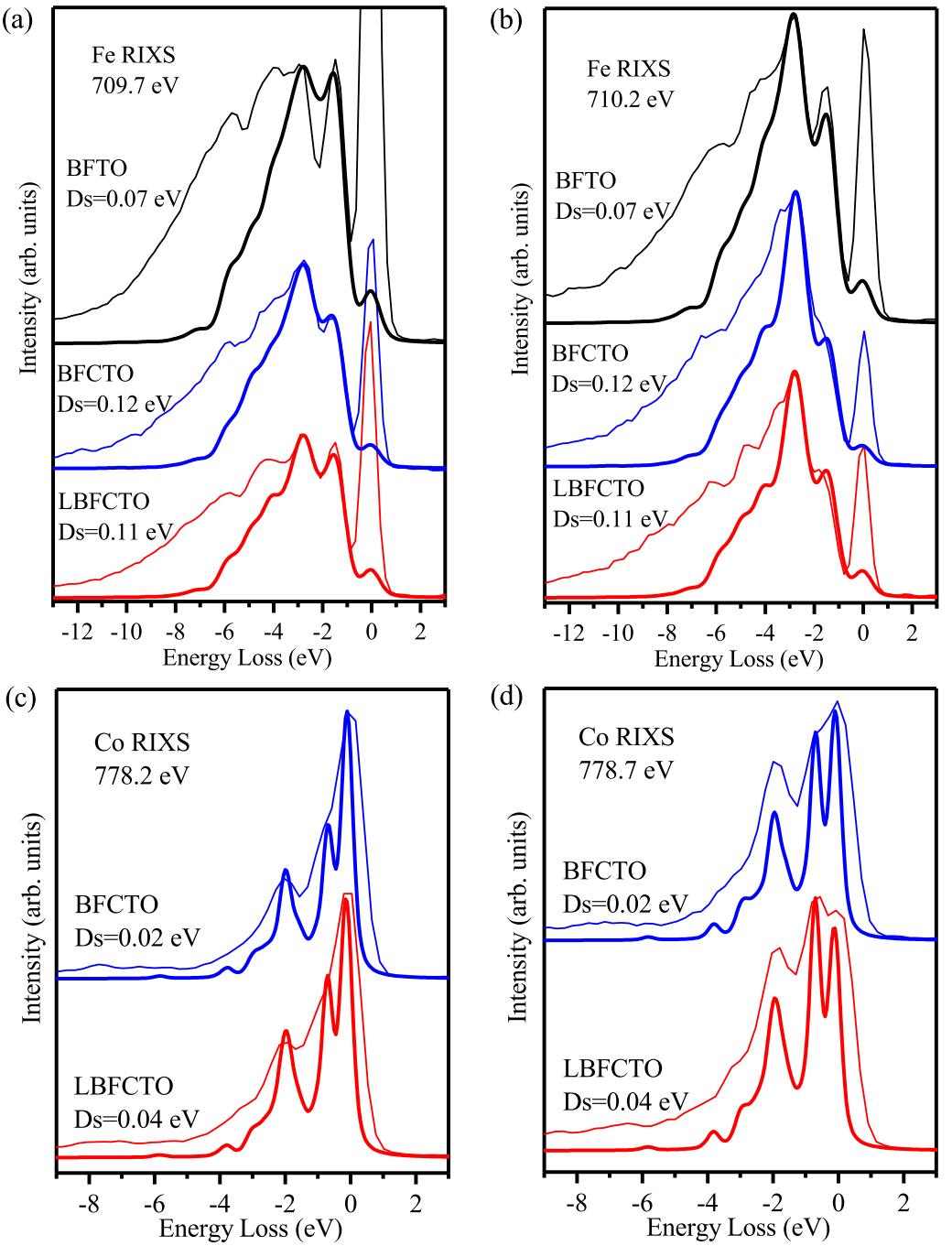

FIG. 5. Simulated Fe^{3+} (top panel) and Co^{2+} (bottom panel) L-edge RIXS spectra (thick curves) as a function of Ds in comparison with the experimental spectra (thin curves) of BFTO, BFCTO, and LBFCTO films at the incident photon energy of (a) 709.7, (b) 710.2, (c) 778.2, and (d) 778.7 eV. The intensities of simulated spectra are all rescaled for clarity.

octahedral ligand field. Thus we introduce a small tetragonal crystal-field splitting to oxygen octahedra and investigate the consequent influences on the RIXS excitations.

Figure 5 shows the simulated Fe^{3+} and Co^{2+} L-edge RIXS spectra in comparison with the experimental spectra of BFTO, BFCTO, and LBFCTO films at selected incident photon energies (detailed comparison of experimental and simulated Fe and Co RIXS spectra can also be found in the Supplemental Material [36]). For Fe^{3+} RIXS simulations, the crystal-field parameters $10Dq$ and Ds ($Dt = 0$ for all simulations) are fitted to the experimental spectra, which yields $10Dq = 1.6$ eV for all films. This $10Dq$ value is consistent with the previous report of Fe^{3+} in oxygen octahedra [31]. In order to reach good agreement with experimental data, the Ds value, which is used to introduce the tetragonal crystal-field splitting, has to be tuned. The Ds values for BFTO, BFCTO, and LBFCTO films are then fitted to be 0.07, 0.12, and 0.11 eV, respectively. For Co^{2+} RIXS simulations, the $10Dq$ value is fitted to be 0.7 eV for both BFCTO and LBFCTO films while Ds is determined to be about 0.02 eV for BFCTO

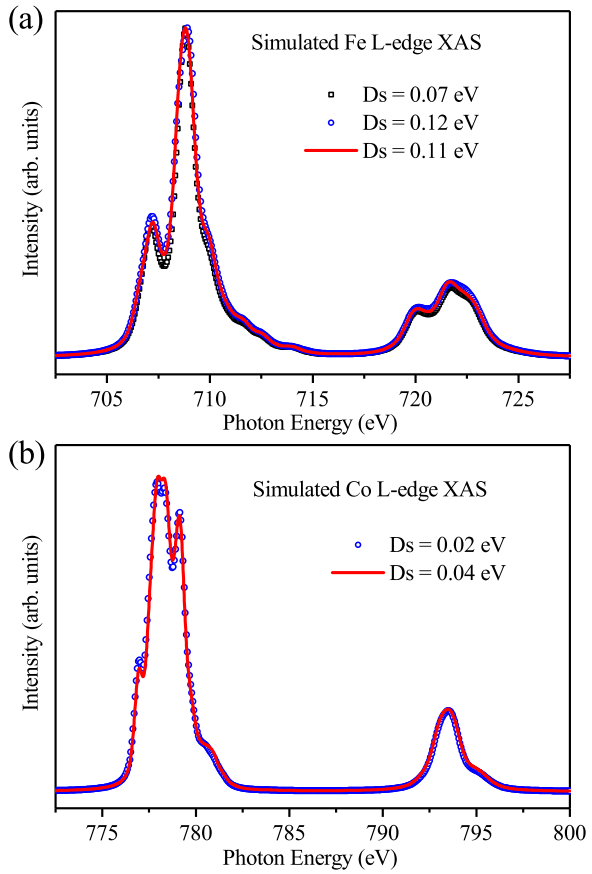

FIG. 6. Simulated (a) Fe^{3+} (top panel) and (b) Co^{2+} L-edge (bottom panel) XAS spectra as a function of Ds. All the spectra are normalized to the maximum intensity for clarity.

and 0.04 eV for LBFCTO. This $10Dq$ value is close to that in previous reports [32,33,37]. The simulated RIXS spectra well reproduce the energy positions and relative intensity behavior of crystal-field excitations in the experimental RIXS spectra. The simulated Co RIXS spectra are in better agreement with the experimental ones, whereas the simulated Fe RIXS spectra display noticeable discrepancy at the high-energy side. This is due to the charge-transfer excitations between O^{2-} and Fe^{3+} that are not included in the simulations. On the other hand, the charge-transfer excitations in Co are weaker and are located at much higher energy, further away from the crystal-field excitations. The exclusion of charge-transfer effect in simulation can limit the number of semiempirical parameters used in RIXS simulations and lead to more robust determination of crystal-field parameters for the compounds under study [33].

Our RIXS simulations demonstrate that the crystal-field splitting of FeO_6 and CoO_6 octahedra are modified by Co and La doping. The doping of Co and La could influence the lattice structures because of changed bond lengths. Besides, the dopants can also induce pure electronic effect such as changing the crystal-field potential [38]. These two effects are mutually related and both of them could be the causes for the modified crystal-field splitting. Separating the contribution of these two effects may require first-principle calculations while such calculations are very challenging considering the large unit cells of these compounds. Relating first-principle calculations to RIXS spectral shapes is far more challenging, which might be an interest for future study, whereas the semiempirical multiplet calculations enable the direct comparison between XAS/RIXS spectra and electronic structures of complex compounds.

For comparison, we have also carried out the XAS simulations using the same parameters as in the RIXS simulations. The Gaussian broadening for instrumentation resolution is set to 0.15 eV for both Fe and Co. The Lorentzian broadening for Fe is 0.3 eV at the L_3 edge and 0.4 eV at the L_2 edge and this value for Co is 0.15 and 0.4 eV, respectively. Figure 6 shows the simulated L-edge XAS spectra of Fe^{3+} and Co^{2+} as a function of Ds. The simulated XAS of Fe^{3+} is quite similar to the experimental spectra of BFTO, BFCTO, and LBFCTO. Both samples have Co^{3+} contributions and we expect more Co^{3+} ions in the LBFCTO film than in the BFCTO film. The existence of Co^{3+} will increase the peak intensity at 779.1 eV. Here, the Co^{2+} XAS simulations are displayed and they reproduce the spectral profiles and peak positions of the experimental spectra of BFCTO and LBFCTO. These observations support that the parameters used in the RIXS simulations are correctly chosen. Besides, for all XAS simulations, only very small changes can be observed with different Ds parameters. This echoes our previous statement that the core-hole lifetime broadening in Fe and Co L-edge XAS spectra hinders the detailed studies of subtle spectral changes resulting from the dopants.

IV. CONCLUSION

In summary, we have performed XAS and RIXS studies at both Fe and Co L edges on BFTO, BFCTO, and LBFCTO epitaxial thin films. The XAS measurements show the Fe ions have a higher valence state than Co ions and the reduced oxygen vacancy concentration due to La doping. The RIXS measurements revealed the modified electronic structures of these compounds as a result of Co and La doping. The experimental RIXS spectra are compared with simulations based on atomic multiplet plus crystal-field theory. The RIXS simulations suggest that the observed variations of the electronic structures can be attributed to the modified crystal-field potential of FeO_6 and CoO_6 octahedra. The crystal-field parameter $10Dq$ for FeO_6 octahedra is fitted to be 1.6 eV for all thin films while this value for CoO_6 octahedra is 0.7 eV for BFCTO and LBFCTO. This implies the Fe-O bonds are stronger than the Co-O bonds, which could be related to the higher valence state of Fe ions. Furthermore, the RIXS studies demonstrated the dependence of crystal-field splitting on the doping of Co and La. These observations suggest that RIXS can be the powerful tool to investigate the subtle changes in electronic structures of perovskite oxides.

ACKNOWLEDGMENTS

This work was supported by the National Key Research and Development Program of China (2016YFA0401004), the External Cooperation Program of BIC, Chinese Academy of Sciences (Grant No. 211134KYSB20130017), the Key

Research Program of Chinese Academy of Sciences (KGZD-EW-T06) and Hefei Science Center, Chinese Academy of Sciences (2016HSC-IU004). The Advanced Light Source is supported by the Director, Office of Science, Office of Basic Energy Sciences, of the U.S. Department of Energy under Contract No. DE-AC02-05CH11231.

[1] X. Mao, W. Wang, X. Chen, and Y. Lu, Appl. Phys. Lett. **95**, 082901 (2009).
[2] H. Zhao, K. Cai, Z. Cheng, T. Jia, H. Kimura, Z. Ma, Q. Fu, Z. Huang, T. Matsumoto, T. Tohei, N. Shibata, and Y. Ikuhara, Adv. Electron. Mater. **3**, 1600254 (2017).
[3] T. Jia, H. Kimura, Z. Cheng, H. Zhao, Y.-H. Kim, M. Osada, T. Matsumoto, N. Shibata, and Y. Ikuhara, NPG Asia Mater. **9**, e349 (2017).
[4] Y. Yun, X. Zhai, C. Ma, H. Huang, D. Meng, Z. Cui, J. Wang, Z. Fu, R. Peng, and G. J. Brown, Appl. Phys. Express **8**, 054001 (2015).
[5] J. M. Rondinelli and C. J. Fennie, Adv. Mater. **24**, 1961 (2012).
[6] X. Zhai, L. Cheng, Y. Liu, C. M. Schleputz, S. Dong, H. Li, X. Zhang, S. Chu, L. Zheng, J. Zhang, A. Zhao, H. Hong, A. Bhattacharya, J. N. Eckstein, and C. Zeng, Nat. Commun. **5**, 4283 (2014).
[7] E. Bousquet, M. Dawber, N. Stucki, C. Lichtensteiger, P. Hermet, S. Gariglio, J. M. Triscone, and P. Ghosez, Nature **452**, 732 (2008).
[8] A. Y. Borisevich, H. J. Chang, M. Huijben, M. P. Oxley, S. Okamoto, M. K. Niranjan, J. D. Burton, E. Y. Tsymbal, Y. H. Chu, P. Yu, R. Ramesh, S. V. Kalinin, and S. J. Pennycook, Phys. Rev. Lett. **105**, 087204 (2010).
[9] G. Song and W. Y. Zhang, Phys. Rev. B **94**, 064409 (2016).
[10] M. Shatnawi, E. S. Bozin, J. F. Mitchell, and S. J. L. Billinge, Phys. Rev. B **93**, 165138 (2016).
[11] D. Yang, L. L. Wei, X. L. Chao, Z. P. Yang, and X. Y. Zhou, Phys. Chem. Chem. Phys. **18**, 7702 (2016).
[12] J. Li, L. Sun, P. M. Shenai, J. Wang, H. Zheng, and Y. Zhao, J. Alloys Compd. **649**, 973 (2015).
[13] A. Kotani and S. Shin, Rev. Mod. Phys. **73**, 203 (2001).
[14] L. J. P. Ament, M. van Veenendaal, T. P. Devereaux, J. P. Hill, and J. van den Brink, Rev. Mod. Phys. **83**, 705 (2011).
[15] Z. Liu, J. Yang, X. W. Tang, L. H. Yin, X. B. Zhu, J. M. Dai, and Y. P. Sun, Appl. Phys. Lett. **101**, 122402 (2012).
[16] J. Yang, W. Tong, Z. Liu, X. B. Zhu, J. M. Dai, W. H. Song, Z. R. Yang, and Y. P. Sun, Phys. Rev. B **86**, 104410 (2012).
[17] C. M. Raghavan, J. W. Kim, J. Y. Choi, S. S. Kim, and J.-W. Kim, J. Sol-Gel Sci. Technol. **73**, 83 (2014).
[18] J. Yang, L. H. Yin, Z. Liu, X. B. Zhu, W. H. Song, J. M. Dai, Z. R. Yang, and Y. P. Sun, Appl. Phys. Lett. **101**, 012402 (2012).
[19] C. M. Raghavan, J. W. Kim, J.-W. Kim, and S. S. Kim, Ceram. Int. **40**, 10649 (2014).
[20] C. Murugesan Raghavan, J. Won Kim, J. Ya Choi, J.-W. Kim, and S. Su Kim, Ceram. Int. **41**, 3277 (2015).
[21] Z. Cui, H. Xu, Y. Yun, J. Guo, Y.-D. Chuang, H. Huang, D. Meng, J. Wang, Z. Fu, R. Peng, R. J. Knize, G. J. Brown, X. Zhai, and Y. Lu, J. Appl. Phys. **120**, 084101 (2016).
[22] Y. Yun, C. Ma, X. Zhai, H. Huang, D. Meng, J. Wang, Z. Fu, R. Peng, G. J. Brown, and Y. Lu, Appl. Phys. Lett. **107**, 011602 (2015).
[23] C. L. Chen, C. L. Dong, J. L. Chen, J. H. Guo, W. L. Yang, C. C. Hsu, K. W. Yeh, T. W. Huang, B. H. Mok, T. S. Chan, J. F. Lee, C. L. Chang, S. M. Rao, and M. K. Wu, Phys. Chem. Chem. Phys. **13**, 15666 (2011).
[24] L. Vayssieres, C. Sathe, S. M. Butorin, D. K. Shuh, J. Nordgren, and J. H. Guo, Adv. Mater. **17**, 2320 (2005).
[25] M. Magnuson, S. M. Butorin, J. H. Guo, and J. Nordgren, Phys. Rev. B **65**, 205106 (2002).
[26] H. J. Liu, J. H. Guo, Y. D. Yin, A. Augustsson, C. L. Dong, J. Nordgren, C. L. Chang, P. Alivisatos, G. Thornton, D. F. Ogletree, F. G. Requejo, F. de Groot, and M. Salmeron, Nano Lett. **7**, 1919 (2007).
[27] Y. Luo, H. Agren, F. Gelmukhanov, J. H. Guo, P. Skytt, N. Wassdahl, and J. Nordgren, Phys. Rev. B **52**, 14479 (1995).
[28] L. C. Duda, J. Nordgren, G. Drager, S. Bocharov, and T. Kirchner, J. Electron. Spectrosc. Relat. Phenom. **110-111**, 275 (2000).
[29] C. Monney, A. Uldry, K. J. Zhou, A. Krzton-Maziopa, E. Pomjakushina, V. N. Strocov, B. Delley, and T. Schmitt, Phys. Rev. B **88**, 165103 (2013).
[30] W. L. Yang, A. P. Sorini, C. C. Chen, B. Moritz, W. S. Lee, F. Vernay, P. Olalde-Velasco, J. D. Denlinger, B. Delley, J. H. Chu, J. G. Analytis, I. R. Fisher, Z. A. Ren, J. Yang, W. Lu, Z. X. Zhao, J. van den Brink, Z. Hussain, Z. X. Shen, and T. P. Devereaux, Phys. Rev. B **80**, 014508 (2009).
[31] L. A. Marusak, R. Messier, and W. B. White, J. Phys. Chem. Solids **41**, 981 (1980).
[32] M. M. van Schooneveld, R. Kurian, A. Juhin, K. Zhou, J. Schlappa, V. N. Strocov, T. Schmitt, and F. M. F. de Groot, J. Phys. Chem. C **116**, 15218 (2012).
[33] B. Liu, R. P. Wang, E. N. Glass, C. L. Hill, T. Cuk, J. Okamoto, D. J. Huang, M. M. van Schooneveld, and F. M. de Groot, Inorg. Chem. **55**, 10152 (2016).
[34] F. de Groot, Coord. Chem. Rev. **249**, 31 (2005).
[35] M. Garcia-Guaderrama, L. Fuentes-Montero, A. Rodriguez, and L. Fuentes, Integr. Ferroelectr. **83**, 41 (2006).
[36] See Supplemental Material at http://link.aps.org/supplemental/10.1103/PhysRevB.95.205102 for detailed comparison of experimental and simulated Fe and Co RIXS spectra.
[37] Z. Cui, C. Xie, X. Feng, N. Becknell, P. Yang, Y. Lu, X. Zhai, X. Liu, W. Yang, Y. D. Chuang, and J. Guo, J. Phys. Chem. Lett. **8**, 319 (2017).
[38] M. Moretti Sala, M. Rossi, S. Boseggia, J. Akimitsu, N. B. Brookes, M. Isobe, M. Minola, H. Okabe, H. M. Rønnow, L. Simonelli, D. F. McMorrow, and G. Monaco, Phys. Rev. B **89**, 121101 (2014).